Acta Crystallographica Section B
Structural Science
ISSN 0108-7681

Structural analysis of perovskite $LaCr_{1-x}Ni_xO_3$ by Rietveld refinement of X-ray powder diffraction data

J. Yang

Fachbereich Physik, Universität Dortmund, 44221 Dortmund, Germany

Correspondence e-mail: jieyang@e3.physik.uni-dortmund.de

Received 5 December 2007
Accepted 29 February 2008

The crystal structure of perovskite $LaCr_{1-x}Ni_xO_3$ ($0 \leq x \leq 1.0$) has been systematically investigated by analyzing X-ray powder-diffraction data taken at room temperature. Rietveld refinement has confirmed the structural evolution from the orthorhombic phase (*Pbnm*, $Z = 4$) to the two-phase (the orthorhombic and the rhombohedral phases) region around $x = 0.7$, then to the rhombohedral ($R\bar{3}c$, $Z = 2$) phase for $0.8 \leq x \leq 1.0$. The lattice parameters are also obtained in the refinement process. The results are discussed in terms of reduced Cr/Ni—O bond length with increasing Ni-doping level, leading to an increased tolerance factor caused by the substitution of smaller Ni^{3+} ($R_{Ni^{3+}} = 0.60$ Å, six-coordinate) ions for larger Cr^{3+} ($R_{Cr^{3+}} = 0.615$ Å, six-coordinate) ions.

1. Introduction

Rare-earth perovskite oxides, ABO_3 (A is a lanthanide or alkaline earth metal and B is a 3*d* transition metal), are found to be very useful in a wide range of applications, such as catalysts, electrocatalysts and electronic ceramics (Tejuca & Fierro, 1993). Among the perovskite series of $LaMO_3$ (M = Cr, Mn, Fe, Co and Ni), only $LaCrO_3$ has the stability required for use as a fuel-side electrode (Steele *et al.*, 1990). A wide range of possible substitutions at both the La and the Cr sites in the perovskite $LaCrO_3$ allows the tailoring of electronic, thermodynamic and catalytic properties for specific applications. As a result, compounds $La_{1-x}D_xCrO_3$ (D is a divalent element such as Ca and Sr; Feduska & Isenberg, 1983; Minh, 1993; Mori *et al.*, 1999; Tanasescu *et al.*, 2003; Duran *et al.*, 2004) and $LaCr_{1-x}M_xO_3$ (M = Co and Ni; Kononyuk *et al.*, 1986; Tolochko, Fjellvåg *et al.*, 1987; Tolochko, Kononyuk *et al.*, 1987; Tilset *et al.*, 1994, 1995; Höfer & Schmidberger, 1994; Höfer & Kock, 1993; Ganguly *et al.*, 1984; Stojanović, Haverkamp *et al.*, 1997; Stojanović, Mims *et al.*, 1997; Zhang *et al.*, 1997; Vovk *et al.*, 2005) have recently received much attention as electrocatalytic materials, including electrode materials or interconnections in solid oxide–electrolyte fuel cells. Although a number of investigations on the catalytic activity, the conductivity and the surface structure of $LaCr_{1-x}Ni_xO_3$ have been reported (Kononzuk *et al.*, 1986; Tolochko *et al.*, 1987; Höfer & Schmidberger, 1994; Ganguly *et al.*, 1984; Stojanović, Haverkamp *et al.*, 1997; Stojanović, Mims *et al.*, 1997; Zhang *et al.*, 1997; Vovk *et al.*, 2005), to the best of our knowledge, there are few reports on the systematic structural studies of $LaCr_{1-x}Ni_xO_3$. Moreover, some inconsistent results have been released concerning the structural phase transition for $LaCr_{1-x}Ni_xO_3$ compounds. Höfer & Kock (1993) and Ganguly *et al.* (1984) suggested that the structural transition occurred in the range $x = 0.5$–0.65. Later, Stojanović, Haver-

Table 1
Positional parameters for the orthorhombic, rhombohedral and cubic structures, used in the structural refinement.

O1: apical oxygen; O2: basal plane oxygen.

Space group	Atom	Position	Atomic coordinates
Pbnm	La	4(*c*)	$x, y, \frac{1}{4}$
	Cr/Ni	4(*a*)	0, 0, 0
	O1	4(*c*)	$x, y, \frac{1}{4}$
	O2	8(*d*)	x, y, z
$R\bar{3}c$	La	6(*a*)	$0, 0, \frac{1}{4}$
	Cr/Ni	6(*b*)	0, 0, 0
	O	18(*e*)	$x, 0, \frac{1}{4}$
$R\bar{3}c$	Cr	12(*c*)	$0, 0, z$
(Cr_2O_3)	O	18(*e*)	$x, 0, \frac{1}{4}$
*Fm*3*m*	Ni	1(*a*)	0, 0, 0
(NiO)	O	1(*b*)	$\frac{1}{2}, \frac{1}{2}, \frac{1}{2}$

kamp *et al.* (1997) found that the transition between orthorhombic *Pnma* and rhombohedral $R\bar{3}c$ structures took place at $x \simeq 0.6$. However, Zhang *et al.* (1997) reported the structural transition from the orthorhombic *Pbnm* to the rhombohedral $R\bar{3}m$ phase at $x = 0.6$–0.7. Based on the previous reports, it was summarized that the crystal structures of $LaCr_{1-x}Ni_xO_3$ seemed to be less characterized, and furthermore some important structural information, including the atomic coordinates, the Cr/Ni—O bond length and Cr/Ni—O—Cr/Ni bond angle, were still missing. We, therefore, have carried out a systematic structural study on the $LaCr_{1-x}Ni_xO_3$ compounds by applying the Rietveld refinement technique to the X-ray powder-diffraction data, and discussed the physical origin of the structural transition from the orthorhombic *Pbnm* to the rhombohedral $R\bar{3}c$ phase.

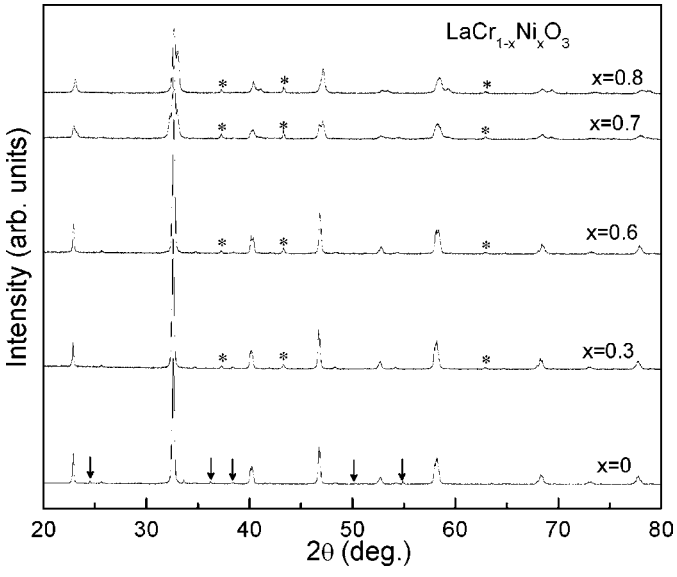

Figure 1
XRD patterns of the $LaCr_{1-x}Ni_xO_3$ compounds. A few very weak peaks are due to the traces of Cr_2O_3 and NiO, as indicated by arrows and asterisks, respectively.

2. Experimental

$LaCr_{1-x}Ni_xO_3$ (x = 0, 0.1, 0.3, 0.5, 0.6, 0.7, 0.8, 0.9 and 1.0) samples were synthesized using the citrate-gel technique (Verelst *et al.*, 1993), since this technique can enhance the density and the phase homogeneity of samples at lower sintering temperatures. The starting materials were ethylene glycol (99%), citric acid (99.5%), lanthanum oxide (La_2O_3: 99.99%), chromium(III) nitrate nonahydrate [$Cr(NO_3)_3{\cdot}9H_2O$] and nickel(II) nitrate hexahydrate [$Ni(NO_3)_2{\cdot}6H_2O$]. The La_2O_3 powders were heated at 1073 K to remove the pre-adsorbed water and carbon dioxide before dissolving in diluted nitric acid. The heat-treated La_2O_3 powders were dissolved in diluted nitric acid with added citric acid, followed by the addition of stoichiometric amounts of $Cr(NO_3)_3{\cdot}9H_2O$ and $Ni(NO_3)_2{\cdot}6H_2O$ dissolved in distilled water with continuous stirring. Ethylene glycol was then added to make a complex solution. After all the reactants had been completely dissolved, the solution was put on a hot plate to make a gel. The gel was dried at 523 K for 2 h, and a dry foamed resin was obtained. This resin was then ground and calcined at 873 K to remove the remaining organics and to decompose the nitrates of the gel. The powders obtained were ground, pelletized and sintered at 1673 K for 24 h, and then the furnace was slowly cooled down to room temperature.

The X-ray diffraction (XRD) data were collected at room temperature using a Philips X'Pert PRO X-ray diffractometer with a Bruker goniometer (goniometer radius of 240 mm) and with Cu $K\alpha$ radiation. The data were collected with a scan step of 0.017° and a count time of 10 s at each step over the angular range $20 < 2\theta < 80°$. The structural calculations were performed using Rietveld's method using the *Rietica* computer program by Howard & Hunter (1997). A polynomial function with four parameters was used to fit the background. The isotropic atomic displacement (U_{iso}) parameters for all atoms were assumed to have values of 0.6 Å, and the profiles have been fitted by using a Voigt peak-shape function.

3. Results and discussion

Fig. 1 shows some of the XRD patterns of $LaCr_{1-x}Ni_xO_3$ sample at room temperature. It is found that traces of the second-phase Cr_2O_3 (< 5%), denoted by arrows in the XRD pattern, are evident in the sample with $x = 0$. Meanwhile, for the samples with $0.1 \leq x \leq 1.0$, different traces of the second-phase NiO, denoted by asterisks in the XRD pattern, are observed. Although it can be seen that the diffraction peaks of NiO become more evident as the Ni doping increases, the samples can be considered to be nearly single phase, since the amount of the second phase is below 5%. It is worth noting that the crystal structure changes at *ca* $x = 0.8$. This point will be discussed later.

In order to investigate the crystal structure of $LaCr_{1-x}Ni_xO_3$ samples more closely, we deduced the structural parameters of samples which were refined using the standard Rietveld technique. The atomic positions and coordinates of different structures and space groups, obtained during the

Table 2
Refined structural parameters of $LaCr_{1-x}Ni_xO_3$ ($0 \leq x \leq 1$) at room temperature.

Parameter	$x = 0$ *Pbnm*	$x = 0.3$ *Pbnm*	$x = 0.6$ *Pbnm*	$x = 0.7$ *Pbnm*	$R\bar{3}c$	$x = 0.8$ $R\bar{3}c$	$x = 0.9$ $R\bar{3}c$	$x = 1.0$ $R\bar{3}c$
a (Å)	5.5133 (1)	5.5094 (9)	5.5180 (1)	5.5032 (2)	5.4831 (2)	5.4809 (3)	5.4747 (6)	5.4561 (1)
b (Å)	5.4759 (6)	5.4740 (1)	5.4735 (3)	5.4612 (6)	5.4831 (2)	5.4809 (3)	5.4747 (6)	5.4561 (1)
c (Å)	7.7585 (9)	7.7536 (8)	7.7529 (5)	7.7407 (7)	13.2091 (3)	13.2070 (5)	13.1990 (3)	13.1432 (3)
V (Å^3)	234.237 (3)	233.843 (5)	234.163 (4)	232.636 (1)	343.924 (1)	343.586 (4)	342.600 (2)	338.844 (9)
Space group	*Pbnm*	*Pbnm*	*Pbnm*	*Pbnm*	$R\bar{3}c$	$R\bar{3}c$	$R\bar{3}c$	$R\bar{3}c$
Z	4	4	4	4	2	2	2	2
No. of parameters	31	28	23	25	25	25	25	18
Second phase	Cr_2O_3	NiO	NiO	NiO	$R\bar{3}C$	NiO	NiO	NiO
Fraction (%)	3.75	2.61	2.97	3.42	21.48	3.77	3.90	4.13
R_p	0.0897	0.0790	0.0674	0.0871		0.0723	0.0948	0.1057
R_{wp}	0.1220	0.0996	0.0863	0.1168		0.0928	0.1157	0.1239
χ^2	1.82	1.79	1.62	3.08		1.95	2.13	2.21
La								
x	0.4971 (5)	0.4979 (8)	0.4926 (4)	0.4983 (5)				
y	0.0180 (7)	0.0203 (8)	0.0242 (1)	0.0206 (9)				
O1								
x	0.5594 (3)	0.5744 (6)	0.5656 (2)	0.5791 (3)	0.5523 (3)	0.5517 (4)	0.5507 (3)	0.5501 (2)
y	0.4993 (6)	0.4956 (1)	0.4865 (4)	0.5009 (5)				
O2								
x	0.2249 (1)	0.2324 (4)	0.2327 (1)	0.2480 (3)				
y	0.2688 (2)	0.3082 (1)	0.2863 (3)	0.3032 (1)				
z	0.0376 (7)	0.0236 (5)	0.0286 (8)	0.0201 (4)				
(Cr_2O_3)								
Cr								
z	0.3518 (3)							
O								
x	0.3194 (8)							
Cr/Ni—O1 ×2 (Å)	1.9671 (7)	1.9815 (2)	1.8950 (1)	1.9835 (3)				
Cr/Ni—O2 ×2 (Å)	1.9468 (3)	2.1260 (1)	2.0387 (6)	2.1513 (5)				
Cr/Ni—O2 ×2 (Å)	1.9971 (4)	1.8191 (2)	1.9732 (3)	1.7615 (2)				
(Cr/Ni—O) (Å)	1.9703 (5)	1.9755 (1)	1.9690 (3)	1.9654 (3)	1.9490 (1)	1.9481 (4)	1.9453 (3)	1.9384 (5)
Cr—O1—Cr ×2 (°)	160.82	156.06	158.42	154.65				
Ni—O1—Ni ×2 (°)								
Cr—O2—Cr ×4 (°)	160.23	159.63	162.18	164.30				
Ni—O2—Ni ×4 (°)								
⟨Cr—O—Cr⟩ (°)	160.43	158.44	160.93	161.08	163.08	163.27	163.59	163.78
⟨Ni—O—Ni⟩ (°)								

refinement process, are summarized in Table 1, and the structural parameters, obtained are listed in Table 2.[1] Moreover, the ratios of Cr/Ni were also refined and it was found that the Cr/Ni ratios were rather stable and almost consistent with the nominal ratio of $1 - x/x$. The Rietveld refinement yielded satisfactory results, based on the consideration of lower-profile R_p and weighted-profile R_{wp} values, as shown in Table 2. The quantities employed to estimate the agreement between the observations and the models during the course of the refinement are as follows:

(i) profile

$$R_p = \frac{\sum |y_{io} - y_{ic}|}{\sum y_{io}}, \tag{1}$$

(ii) weighted profile

$$R_{wp} = \left[\frac{\sum w_i (y_{io} - y_{ic})^2}{\sum w_i y_{io}^2}\right]^{1/2}, \tag{2}$$

(iii) goodness of fit

$$\chi^2 = \frac{\sum w_i (y_{io} - y_{ic})^2}{M - P}, \tag{3}$$

where y_{io} is the set of observed diffraction intensities collected at each step across the pattern, y_{ic} is the set of corresponding calculated values, w_i, *i.e.* n/y_{ic} (n is the number of detectors contributing to the step intensity average) is the weight assigned to each observation, M is the number of observations (*i.e.* the total number of y_{io}s when the background is refined) and P is the number of adjusted parameters.

The experimental and calculated XRD results of the sample with $x = 0$ are shown in Fig. 2(*a*). As can be seen clearly, $LaCrO_3$ is a two-phase compound composed of the orthorhombic $LaCrO_3$ and the rhombohedral Cr_2O_3. As shown in Table 2, the lattice parameters of $LaCrO_3$ with the space group *Pbnm* are $a = 5.5133$ (1), $b = 5.4759$ (6) and $c = 7.7585$ (9) Å,

[1] Supplementary data for this paper are available from the IUCr electronic archives (Reference: BP5009). Services for accessing these data are described at the back of the journal.

which are close to the published lattice parameters: a = 5.514, b = 5.478 and c = 7.752 Å (JCPDS card No. 71-1231). The lattice parameters found for Cr_2O_3 with the space group $R\bar{3}C$ are also close to the published data: a = 4.958 and c = 13.59 Å (JCPDS card No. 06-0504). Different structural results of $LaCrO_3$ have also been reported: the lattice parameters for $LaCrO_3$ with the space group *Pnma* are a = 5.4771 (4), b = 7.7620 (5) and c = 5.5197 (4) Å (Stojanović, Haverkamp *et al.*, 1997), and with the space group *Pbnm* a = 5.493, b = 5.505 and c = 7.763 Å (Zhang *et al.*, 1997). Zhang *et al.* (1997) confused the lattice parameters obtained for $LaCrO_3$ with those published (JCPDS card No. 33–701) in order to consider them as comparable. The lattice parameters $LaCrO_3$ in Zhang *et al.* (1997) belong to the orthorhombic system with the space group *Pbnm*, whereas the published lattice parameters (JCPDS card No. 33-701) belong to that with the space group *Pnma*.

The weight fraction of the second phase can also be obtained by the refinement. A quantitative analysis can be performed on multi-phase samples using the formalism described by Hill & Howard (1987). In general, the scattering cross-section of the Bragg scattering is proportional to N/V, where N is the number of unit cells contributing to the scattering and V is the unit-cell volume. The scale factor, S, is then proportional to N/V. The weight fraction of phase p is then derived as

$$W_P = \frac{(SZMV)_P}{\sum_i (SZMV)_i}, \qquad (4)$$

where Z is the number of formula units per unit cell, M is the molar mass of the formula unit, and i is an index running over all phases. As shown in Table 2, for $LaCrO_3$, the weight fraction of Cr_2O_3 is 3.75%.

It was found that the diffraction patterns of the $LaCr_{1-x}Ni_xO_3$ samples with $0.1 \leq x \leq 0.6$ could also be refined well using the orthorhombic *Pbnm* phase and the cubic *Fm*3*m* phase of NiO with Ni at (0, 0, 0) and O at (0.5, 0.5, 0.5). Figs. 2(*b*) and (*c*) show the experimental and the calculated XRD results of the $LaCr_{1-x}Ni_xO_3$ sample with x = 0.3 and 0.6, respectively, and the lattice parameters are also listed in Table 2.

For the sample with x = 0.7, we refined the XRD data, excluding the cubic *Fm*3*m* phase of NiO, using three models:

(i) orthorhombic model; R_p = 0.1276 and R_{wp} = 0.1653;

(ii) rhombohedral model; R_p = 0.1578 and R_{wp} = 0.1856;

(iii) orthorhombic + rhombohedral model; R_p = 0.0871 and R_{wp} = 0.1168.

The orthorhombic + rhombohedral model turns out to be the best, because of the smallest values for R_p and R_{wp}. In Fig. 2(*d*), only the fitting, based on the orthorhombic + rhombohedral

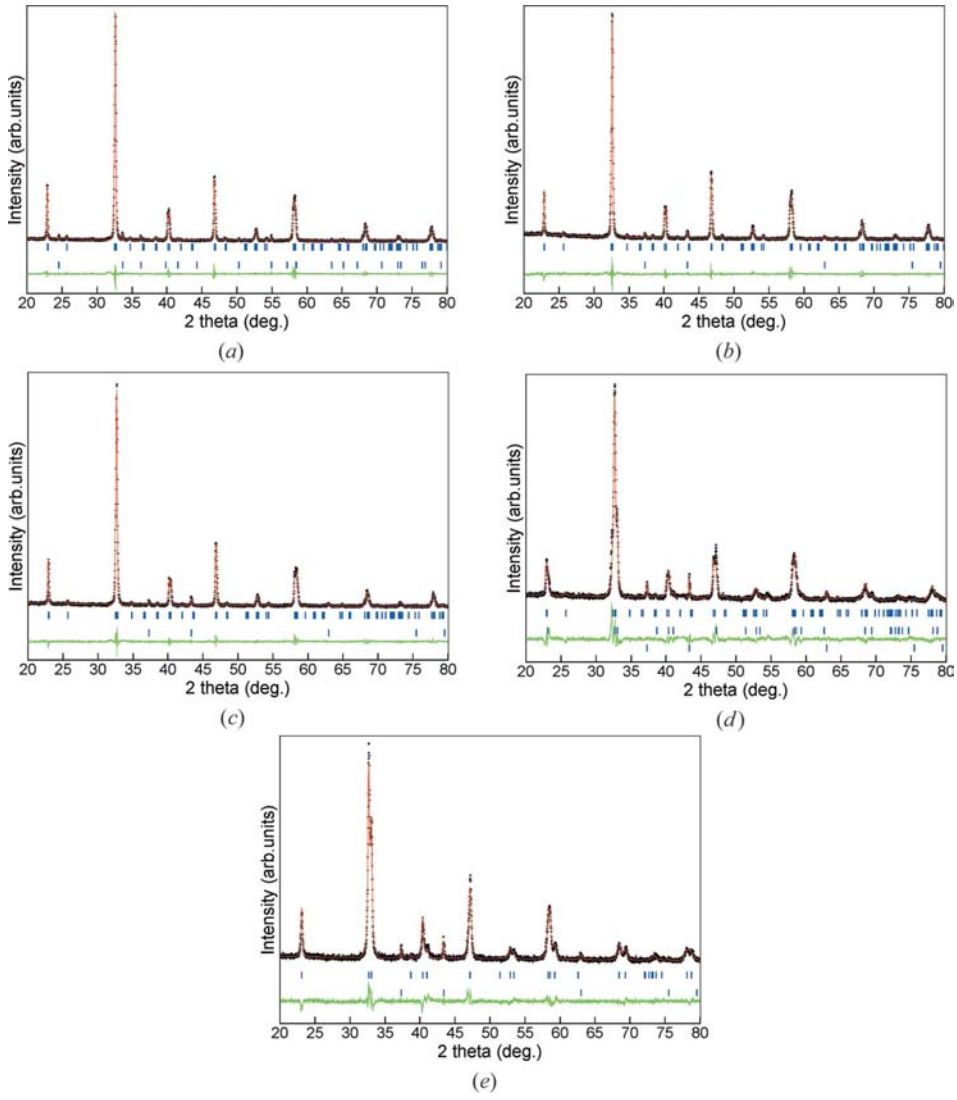

Figure 2
Observed (cross) and calculated (continuous line) profiles of the X-ray powder diffraction for $LaCr_{1-x}Ni_xO_3$. The lowest curve shows the difference between experimental and calculated patterns. (*a*) $LaCrO_3$: the upper and the lower vertical bars indicate the expected reflection positions for the orthorhombic $LaCrO_3$ and the rhombohedral Cr_2O_3, respectively; (*b*) and (*c*) $LaCr_{0.7}Ni_{0.3}O_3$ and $LaCr_{0.4}Ni_{0.6}O_3$, respectively: the upper and the lower vertical bars indicate the expected reflection positions for the orthorhombic $LaCr_{1-x}Ni_xO_3$ and the cubic NiO, respectively; (*d*) $LaCr_{0.3}Ni_{0.7}O_3$: the upper, the middle and the lower vertical bars indicate the expected reflection positions for the orthorhombic $LaCr_{0.3}Ni_{0.7}O_3$, the rhombohedral $LaCr_{0.3}Ni_{0.7}O_3$ and the cubic NiO, respectively; (*e*) $LaCr_{0.2}Ni_{0.8}O_3$: the upper and the lower vertical bars indicate the expected reflection positions for the rhombohedral $LaCr_{0.2}Ni_{0.8}O_3$ and the cubic NiO, respectively.

model, is shown. Therefore, we argue that there are three phases in the $LaCr_{1-x}Ni_xO_3$ sample with $x = 0.7$: the orthorhombic and the rhombohedral phases of $LaCr_{0.3}Ni_{0.7}O_3$, and the cubic phase of NiO. Moreover, according to the quantitative phase analysis, it was found that the concentrations of rhombohedral and cubic phases are 21.48 and 3.42%, respectively, implying that the orthorhombic phase is the major phase of the $LaCr_{0.3}Ni_{0.7}O_3$ sample. Stojanović, Haverkamp *et al.* (1997) mentioned that the transition between orthorhombic and rhombohedral structures was expected to be first order and, therefore, a concentration range for coexistence of the two structural phases should be present, as seen in $LaCr_{1-x}Co_xO_3$ (Tilset *et al.*, 1994). However, the line widths and the compositional resolution for $LaCr_{1-x}Ni_xO_3$ preclude the observation of the coexistence region (Stojanović, Haverkamp *et al.*, 1997). As noticed later, the sample with $x = 0.8$ has only the rhombohedral phase of $LaCr_{1-x}Ni_xO_3$ and the sample with $x = 0.6$ only the orthorhombic one, while the sample with $x = 0.7$ has both phases. Although we cannot pinpoint the exact concentration range for coexistence of the two phases, we, at least, conclude that there is a concentration range of coexistence between $x = 0.6$ and 0.8.

It was found that the diffraction patterns of the $LaCr_{1-x}Ni_xO_3$ samples with $0.8 \leq x \leq 1.0$ could be refined well using the rhombohedral structure and the cubic NiO. As an example, Fig. 2(*e*) shows the experimental and the calculated XRD results of the sample with $x = 0.8$. As seen clearly, the sample with $x = 0.8$ can be refined very well by the rhombohedral $R\bar{3}C$ phase and the cubic $Fm3m$ phase NiO, implying that the crystal structure at room temperature completely changes from the orthorhombic ($Pbnm$, $Z = 4$) to the rhombohedral phase ($R\bar{3}c$, $Z = 2$) at $x \simeq 0.8$. It should be noted here that this observation is different from other reports ($x = 0.5$–0.65; Höfer & Kock, 1993). It is well known that one of the possible origins for the lattice distortion of perovskites structures is the deformation of NiO_6 octahedra, originating from the Jahn–Teller (JT) effect which is related directly to the concentration of Ni^{3+} JT ions. However, $LaNiO_3$ is a metallic conductor with a transfer energy of the JT-e_g electrons larger than the JT stabilization energy, and thus the JT distortion of oxygen octahedra surrounding the Ni^{3+} ion is suppressed (Bednorz & Müller, 1988). Therefore, the observed lattice distortion should be caused by only the size mismatch between the La—O and the Ni/Cr—O layers, which is governed by the tolerance factor t, defined as $t \equiv (r_A + r_O)/2^{1/2}(r_B + r_O)$ (Goldschmidt, 1926), where r_i ($i = A$, B or O) represents the average ionic radius of each element. It is well known that a certain internal stress is introduced into the structure when there is a size mismatch between A and B sites. The internal stress can be partially relieved by the structural distortions. The cubic structure is distorted either by atom B moving off center in its octahedra or by the cage collapsing owing to the rotation of BO_6 octahedra. As t is close to 1, the cubic perovskite structure is formed. As t decreases, the lattice structure transforms to the rhombohedral ($R\bar{3}c$), and then to the orthorhombic ($Pbnm$) structure, in which the bending of the B—O—B bond increases and the bond angle deviates from 180°. For the present system, the observed lattice distortion arises from the partial replacement of Cr by Ni because of the fixed ionic radius of the A site. The doping of a larger ion at the B site should compress the neighboring B—O bonds and result in a decrease in the B—O—B bond angle, *i.e.* an increase in the B—O bond length. On the contrary, a smaller ion at the B site should lead to a decrease of the B—O bond length. The standard six-coordinate ionic radii are 0.60 Å for Ni^{3+} and 0.615 Å for Cr^{3+} in perovskite structure compounds (Shannon, 1976). As a result, for $LaCr_{1-x}Ni_xO_3$ samples, the structural transition at room temperature mainly originates from the increase in the tolerance factor t, in which the smaller Ni^{3+} ions are substituted for the larger Cr^{3+} ions, resulting in the reduction of the Cr/Ni—O bond length as the Ni-doping level increases. This is consistent with the refined values of mean Cr/Ni—O bond lengths shown in Table 2.

4. Conclusions

In conclusion, we have investigated the crystal structures of the perovskite $LaCr_{1-x}Ni_xO_3$ ($0 \leq x \leq 1.0$) by applying the Rietveld refinement technique to X-ray powder diffraction data. The concentration range of the coexistence of the orthorhombic and rhombohedral phases is between $x = 0.6$ and 0.8. The crystal structure at room temperature completely changes from the orthorhombic phase ($Pbnm$, $Z = 4$) to the rhombohedral phase ($R\bar{3}c$, $Z = 2$) at $x \simeq 0.8$, resulting from the progressive increase of the tolerance factor t caused by the substitution of the smaller Ni^{3+} ions for the larger Cr^{3+} ions.

References

Bednorz, J. G. & Müller, K. A. (1988). *Rev. Mod. Phys.* **60**, 585–600.
Duran, P., Tartaj, J., Capel, F. & Moure, C. (2004). *J. Eur. Ceram. Soc.* **24**, 2619–2629.
Feduska, W. & Isenberg, A. O. (1983). *J. Powder Source*, **10**, 89–102.
Ganguly, P., Vasanthacharya, N. Y., Rao, C. N. R. & Edwards, P. P. (1984). *J. Solid State Chem.* **54**, 400–406.
Goldschmidt, V. M. (1926). *Naturwissenschaften*, **14**, 477–485.
Hill, R. J. & Howard, C. J. (1987). *J. Appl. Cryst.* **20**, 467–474.
Howard, C. J. & Hunter, B. A. (1997). *Rietica*. Lucas Heights Research Laboratories, Australia.
Höfer, H. E. & Kock, W. F. (1993). *J. Electrochem. Soc.* **140**, 2889–2894.
Höfer, H. E. & Schmidberger, R. (1994). *J. Electrochem. Soc.* **141**, 782–786.
Kononyuk, I. F., Tolochko, S. P. & Surmach, N. G. (1986). *Inorg. Mater.* **22**, 83–86.
Minh, N. Q. (1993). *J. Am. Ceram. Soc.* **76**, 563–588.
Mori, M., Hiei, Y. & Sammes, N. M. (1999). *Solid State Ion.* **123**, 103–111.
Shannon, R. D. (1976). *Acta Cryst.* A**32**, 751–767.
Steele, B. C. H., Middleton, P. H. & Rudkin, R. A. (1990). *Solid State Ion.* **40–41**, 388–393.
Stojanović, M., Haverkamp, R. G., Mims, C. A., Moudallal, H. & Jacobson, A. J. (1997). *J. Catalysis*, **165**, 315–323.
Stojanović, M., Mims, C. A., Moudallal, H., Yang, Y. L. & Jacobson, A. J. (1997). *J. Catalysis*, **166**, 324–332.
Tanasescu, S., Berger, D., Neiner, D. & Totir, N. D. (2003). *Solid State Ion.* **157**, 365–370.

Tejuca, L. J. & Fierro, J. L. J. (1993). *Properties and Applications of Perovskite-Type Oxides.* Dekker: New York.
Tilset, B. G., Fjellvåg, H. & Kjekshus, A. (1994). *Acta Chim. Scand.* **48**, 37–45.
Tilset, B. G., Fjellvåg, H. & Kjekshus, A. (1995). *J. Solid State Chem.* **119**, 271–280.
Tolochko, S. P., Kononyuk, I. F., Lyutsko, V. A. & Zonov, Y. G. (1987). *Inorg. Mater.* **23**, 1342–1345.
Tolochko, S. P., Kononyuk, I. F., Zonov, Y. G. & Ivashkevich, L. S. (1987). *Inorg. Mater.* **23**, 743–746.
Verelst, M., Rangavittal, N., Rao, C. N. & Rousset, A. (1993). *J. Solid State Chem.* **104**, 74–80.
Vovk, G., Chen, X. & Mims, C. A. (2005). *J. Phys. Chem. B*, **109**, 2445–2454.
Zhang, G. J., Liu, R., Yang, Y. & Jia, Y. Q. (1997). *Phys. Status Solidus A*, **160**, 19–27.